Molecular Vision 2021; 27:179-190 <http://www.molvis.org/molvis/v27/179>
Received 4 April 2020 | Accepted 31 March 2021 | Published 2 April 2021

© 2021 Molecular Vision

A novel homozygous missense mutation p.P388S in *TULP1* causes protein instability and retinitis pigmentosa

DaNae R. Woodard,[1] Chao Xing,[2,3,4] Pratyusha Ganne,[5,6] Hanquan Liang,[2] Avinash Mahindrakar,[5] Chandrasekhar Sankurathri,[5] John D. Hulleman,[1,7] V. Vinod Mootha[1,2]

[1]Department of Ophthalmology, University of Texas Southwestern Medical Center, Dallas, Texas, United States; [2]McDermott Center for Human Growth and Development/Center for Human Genetics, University of Texas Southwestern Medical Center, Dallas, TX; [3]Department of Bioinformatics, University of Texas Southwestern Medical Center, Dallas, TX; [4]Department of Population and Data Sciences, University of Texas Southwestern Medical Center, Dallas, TX; [5]Srikiran Institute of Ophthalmology, Kakinada, Andhra Pradesh, India; [6]Department of Ophthalmology, All India Institute Medical Sciences, Mangalagiri, Andhra Pradesh, India; [7]Department of Pharmacology, University of Texas Southwestern Medical Center, Dallas, TX

Purpose: Retinitis pigmentosa (RP) is an inherited retinal disorder that results in the degeneration of photoreceptor cells, ultimately leading to severe visual impairment. We characterized a consanguineous family from Southern India wherein a 25 year old individual presented with night blindness since childhood. The purpose of this study was to identify the causative mutation for RP in this individual as well as characterize how the mutation may ultimately affect protein function.

Methods: We performed a complete ophthalmologic examination of the proband followed by exome sequencing. The likely causative mutation was identified and modeled in cultured cells, evaluating its expression, solubility (both with western blotting), subcellular distribution, (confocal microscopy), and testing whether this variant induced endoplasmic reticulum (ER) stress (quantitative PCR [qPCR] and western blotting).

Results: The proband presented with generalized and parafoveal retinal pigmented epithelium (RPE) atrophy with bone spicule-like pigmentation in the midperiphery and arteriolar attenuation. Optical coherence tomography scans through the macula of both eyes showed atrophy of the outer retinal layers with loss of the ellipsoid zone, whereas the systemic examination of this individual was normal. The proband's parents and sibling were asymptomatic and had normal funduscopic examinations. We discovered a novel homozygous p.Pro388Ser mutation in the *tubby-like protein 1* (*TULP1*) gene in the individual with RP. In cultured cells, the P388S mutation does not alter the subcellular distribution of TULP1 or induce ER stress when compared to wild-type TULP1, but instead significantly lowers protein stability as indicated with steady-state and cycloheximide-chase experiments.

Conclusions: These results add to the list of known mutations in *TULP1* identified in individuals with RP and suggest a possible unique pathogenic mechanism in *TULP1*-induced RP, which may be shared among select mutations in *TULP1*.

Inherited retinal degenerations (IRDs) caused by autosomal dominant, recessive, and X-linked mutations comprise more than 2 million cases of ocular diseases worldwide [1]. The most common IRD, retinitis pigmentosa (RP), affects 1 in 3,000 individuals worldwide and is characterized by the degeneration of retinal photoreceptor cells beginning with the atrophy of rods and the secondary death of cones [2]. Clinical symptoms of RP include night blindness followed by the loss of peripheral, and eventually, central vision [3].

Currently, more than 30 genes have been associated with autosomal recessive RP [4]. Mutations in the *tubby-like protein 1* (*TULP1*; Gene ID: 7287, OMIM: 602280) gene have been shown to contribute to autosomal recessive RP [5-8]. *TULP1* belongs to the tubby-like gene family that encodes for a 542 amino acid cytoplasmic, membrane-associated protein found exclusively in retinal photoreceptor cells [9]. Previously, the TULP1 protein was demonstrated to be required for normal photoreceptor function through promotion of rhodopsin transport and localization from the inner to outer segments [10], potentially in an F-actin-dependent manner [11]. In addition, in vivo studies have confirmed that mice lacking *Tulp1* display early-onset photoreceptor degeneration due to the loss of rods and cones [12]. Recently, Lobo et al. demonstrated that certain RP-associated autosomal recessive missense mutations in the *TULP1* gene can cause the protein to accumulate within the endoplasmic reticulum (ER), leading to prolonged and possibly detrimental ER stress, providing a surprising but speculative molecular mechanism by which mutations in *TULP1* can induce retinal degeneration [13].

Correspondence to: John D. Hulleman, UT Southwestern Medical Center, Department of Ophthalmology, 5323 Harry Hines Blvd., E7.239, Dallas, TX, 75390-9057; (214) 648 3677; FAX: (214) 648 9061; email: John.Hulleman@UTSouthwestern.edu

In the present study, we identified a novel homozygous missense mutation p.Pro388Sser (P338S) in *TULP1* in a consanguineous family from Southern India who presented with autosomal recessive RP. We explored whether the P388S TULP1 mutant demonstrated any differences in solubility, subcellular localization, or activated cellular stress responses. Our observations revealed that there are no differences in transcript levels between P388S and wild-type (WT) *TULP1*, and the P388S mutation does not induce overt ER stress within cells. Furthermore, we found that P388S localized similarly to WT TULP1 in transfected human embryonic kidney (HEK-293A) and human immortalized retinal pigmented epithelial cells (ARPE-19). However, we found that P388S steady-state levels were significantly reduced and that P388S was more rapidly degraded than WT TULP1 through cycloheximide-chase assays. Our results suggest that certain mutations in *TULP1* may affect protein stability, which may, in turn, contribute to RP disease pathogenesis.

METHODS

Study participants: This study was approved by the Institutional Review Board of the Srikiran Institute of Ophthalmology and followed the tenets of the Declaration of Helsinki. The proband and his family members were recruited and examined after informed consent was received. All participants underwent detailed ophthalmologic evaluations including fundus examination by a retina fellowship-trained ophthalmologist.

Exome sequencing: Approximately 4 ml of blood was drawn from each subject by venipuncture and stored in BD Vacutainer blood collection tubes with K2EDTA (Becton Dickinson, Franklin Lakes, NJ) at 4° C. Genomic DNA from peripheral leukocytes was isolated using the QIAsymphony automated DNA extraction system and QIAsymphony DNA Midi Kit (Qiagen, Hilden, Germany) per manufacturer's protocols.

We performed exome sequencing on genomic DNA of the proband. Library construction and target enrichment were performed using the IDT xGen Exome capture kit (Coralville, IA). The libraries were then sequenced to mean 100X on-target depth on an Illumina sequencing platform (San Diego, CA) with 150 base pairs paired-end reads. Sequences were aligned to the human reference genome b37, and variants were called using the Genome Analysis Toolkit (Cambridge, MA) [14] and annotated using SnpEff [15].

We filtered for rare missense, nonsense, splicing, or frameshift homozygous mutations with a minor allele frequency (MAF) less than 0.01 in the 1000 Genomes Project and genome aggregation (gnomAD) databases. Variants with a Genomic Evolutionary Rate Profiling ($GERP^{2+}$) score greater than 2.0 and a Combined Annotation Dependent Depletion (CADD) score greater than 15 were considered. Known RP susceptibility-conferring genes [16] were screened with priority. Sanger sequencing was used to validate variants of interest in the proband and family members.

Generation of TULP1 constructs: The cDNA encoding for WT human *TULP1* was purchased from the DNASU Plasmid Repository (HsCD00820883, Tucson, AZ). To generate the P388S mutation, Q5 site-directed mutagenesis (New England Biolabs, NEB, Ipswich, MA) of full-length human *TULP1* was performed using the following primers: 5′-CGG GCA GAA CTC ACA GCG TGG-3′ and 5′-TTG TCA AAG ACC GTG AAG CGG-3′. To generate the C-terminal green fluorescent protein (GFP)-tagged WT and P388S *TULP1*, Gibson Assembly (HiFi Master Mix, NEB) was used to insert a Kozak sequence (DNA sequence: GCCACC) upstream of the *TULP1* start codon, and a flexible linker (amino acids: GGGGS) separating *TULP1* and enhanced GFP (eGFP). This TULP1-GGGGS-eGFP DNA was inserted into the peGFP-C1 vector backbone via the SalI and NheI restriction sites. All constructs were verified with Sanger sequencing.

Cell culture: Human embryonic kidney (HEK-293A, Life Technologies, Carlsbad, CA) cells were cultured at 37 °C with 5% CO_2 in Dulbecco's minimal essential medium (DMEM) supplemented with high glucose (4.5 g/l, Corning, Corning, NY), 10% fetal bovine serum (FBS, Omega Scientific, Tarzana, CA), and 1% penicillin-streptomycin-glutamine (Gibco, Waltham, MA). For a 24-well plate, cells were plated at a density of 100,000 cells/well, and for a 12-well plate, cells were plated at a density of 180,000–200,000 cells/well. Cells were transfected the following day with either 500 ng (24 well) or 1 µg (12 well) of midi-prepped endotoxin-free plasmid DNA (Qiagen, Germantown, MD) using Lipofectamine 3000 (Life Technologies) according to the manufacturer's protocol. Forty-eight hours after transfection, fresh media was added, and the cells were harvested 24 h later (72 h posttransfection) and processed for western blotting or quantitative PCR (qPCR). As a positive control for some experiments, cells were treated with tunicamycin (an unfolded protein response inducer, 1 µM, 24 h, Sigma cat# T7765, St. Louis, MO) and processed similarly for western blotting or qPCR. Human immortalized RPE (ARPE-19, CRL-2302, American Type Culture Collection, Manassas, VA) cells were cultured in DMEM/F12 media supplemented with 10% FBS (Omega Scientific), HEPES (Corning, Corning, NY), and penicillin/streptomycin and glutamine (PSQ, Gibco, Germantown, MD). For a 24-well plate, ARPE-19 cells were plated at a density of 100,000 cells/well and transfected the following

day with 500 ng of midi-prepped endotoxin-free plasmid DNA (Qiagen) using Lipofectamine 3000 (Life Technologies). All cells used were verified for authenticity using short tandem repeat (STR) profiling (Appendix 1, University of Arizona Genomics Core, Tucson, AZ). Note that STR verification cannot distinguish among different variants of the 293-based cell lines (i.e., 293 versus 293A versus 293T).

Confocal microscopy: A glass-bottom 24-well plate (MatTek Corporation , Ashland, MA) was coated with 1X poly-D-lysine (Sigma Aldrich), rinsed with water, and allowed to dry at room temperature. HEK-293A or ARPE-19 cells were plated at a density of 100,000 cells/well and transfected the following day with 500 ng of midi-prepped endotoxin-free plasmid DNA (Qiagen). Forty-eight hours after transfection, fresh media was added, and 24 h later (72 h post transfection), the cells were washed twice with 1X PBS (Fisher BioReagents, cat# BP2944100, Waltham, MA) followed by incubation with 4% paraformaldehyde (PFA; Electron Microscopy Sciences, Hatfield, PA) for 20 min. After PFA incubation, cells were washed with 1X PBS. For the ARPE-19 cells, the cell nuclei were stained with 300 nM 4',6-diamidino-2-phenylindole (DAPI), dilactate solution (Molecular Probes, Eugene, OR). For membrane staining, the HEK-293A cells were washed twice with 1X PBS, fixed in 4% PFA, permeabilized in 0.1% Triton X-100 for 3 min, and washed again in 1X PBS. Cells were incubated in blocking buffer (1% bovine serum albumin [BSA] in PBS) for 10 min followed by Alexa Fluor™ 633 Phalloidin (1:50 dilution in PBS; Molecular Probes) for 20 min and washed twice with 1X PBS before being imaged using a 63X oil objective on a Leica SP8 confocal microscope (Buffalo Grove, IL).

Western blotting: Cells were washed with Hanks buffered salt solution (HBSS, Corning), lysed with radioimmunoprecipitation assay (RIPA) buffer (Santa Cruz, Dallas, TX) supplemented with Halt protease inhibitor (Pierce, Rockford, IL) and benzonase (Millipore Sigma) for 3–5 min, and spun at maximum speed (21,000 ×g) at 4 °C for 10 min. The soluble supernatant was collected, and the protein was quantified via bicinchoninic assay (BCA) assay (Pierce). The insoluble pellet fractions were further washed in HBSS and centrifuged, and the pellet was resuspended in 1X sodium dodecyl sulfate (SDS) buffer containing 0.83% beta-mercaptoethanol (BME) and sonicated (30% amplitude, pulse 10 s on/off). Thirty micrograms of soluble supernatant were run on a 4–20% Tris-Gly SDS– polyacrylamide gel electrophoresis (PAGE) gel (Life Technologies) alongside the equivalent amount of insoluble protein and transferred onto a nitrocellulose membrane using an iBlot2 device (Life Technologies). After probing for total protein transferred using Ponceau S (Sigma), the membranes were blocked overnight in Odyssey PBS Blocking Buffer (LI-COR, Lincoln, NE). Membranes were then probed with mouse anti-GFP (1:1,000; Santa Cruz, cat #sc-9996), mouse anti-glucose-regulated protein 78 (GRP78, 1:1,000; Santa Cruz, cat #sc-376768), or rabbit anti-β-actin (1:1,000; LI-COR, Lincoln, NE, cat# 926–42210). Blots were imaged on an Odyssey CLx and quantified using ImageStudio (both from LI-COR).

Quantitative PCR: Transfected HEK-293A cells were trypsinized (0.25% Trypsin EDTA, Gibco), quenched with DMEM, and centrifuged at maximum speed (21,000 ×g) at 4 °C for 10 min. Cell pellets were washed with HBSS and centrifuged again, and then RNA extraction from the cell pellets was performed using the Aurum Total RNA Mini Kit (Bio-Rad, Hercules, CA). Four hundred nanograms of RNA were reverse transcribed using qScript cDNA SuperMix (Quanta Bioscience, Beverly, MA) according to vendor recommended parameters (5 min at 25° C, 30 min at 42° C, 5 min at 85° C), and the cDNA was diluted 5X in DNase/RNase-free water. cDNA was amplified with TaqMan Fast Advanced Master Mix (Thermo Fisher; Applied Biosystems, Waltham, MA (cat# 4444963), 20 sec at 95° C [initial denaturation], 1 sec at 95° C, 20 sec at 60° C, 40 cycles). TaqMan probes used were hTULP1 (cat# hs00163236_m1), hHSPA5 (cat# hs00607129_gH), hDNAJB9 (cat# hs01052402_m1), hASNS (cat# hs04186194_m1), and hACTB (cat# hs01060665_g1; Thermo Fisher; Applied Biosystems) and quantification was performed using using QuantStudio 6 Real-Time PCR software (Thermo Fisher; Applied Biosystems).

Cycloheximide-chase assay: Twenty-four hours after transfection with the WT TULP1 eGFP or P388S TULP1 eGFP constructs, the HEK-293A cells were treated in 24-well plates with cycloheximide (25 µM; Alfa Aesar, Haverhill, MA, cat# J66901-03) for 0, 1, 3, 6, and 9 h. Cells were washed with HBSS, harvested at each time point, and then processed for western blotting. Membranes were probed with mouse anti-GFP and rabbit anti-β-actin and imaged/quantified as described above.

RESULTS

Proband from a consanguineous family in Southern India: A 25-year-old man (Study ID: SIO221) born of a consanguineous marriage in Andhra Pradesh, India, an area where we previously identified unique autosomal recessive mutations linked to eye disease [17], presented with a history of night blindness since childhood. Best-corrected visual acuity (BCVA) in both eyes was 20/60. He had no nystagmus. Intraocular pressure and anterior segment examinations were normal. Fundus examination revealed a fairly symmetric generalized and

parafoveal RPE atrophy with bone spicule-like pigmentation in the midperiphery and arteriolar attenuation (Figure 1A,B). The optic nerve head was normal in appearance. Fundus autofluorescence revealed a parafoveal ring of hypoautofluorescence corresponding to the area of RPE atrophy and a patchy decrease in autofluorescence throughout the retina in both eyes (Figure 1C,D). Optical coherence tomography scans through the macula of both eyes showed atrophy of the outer retinal layers with loss of the ellipsoid zone (EZ) and a thin epiretinal membrane (Figure 1E,F). For comparison, an age-matched healthy control patient was imaged using the same modalities (Figure 1G–L). There was no evidence of posterior staphyloma in the patient. The patient's axial lengths were 24.47 mm and 24.25 mm, respectively. Systemic examination was normal. The examined parents and sibling (pedigree shown in Figure 2A) were asymptomatic and had normal funduscopic examinations.

Exome sequencing identifies a novel homozygous mutation in the TULP1 gene: Exome sequencing of the proband, followed by application of filtering criteria (described in Methods and the flowchart provided in Appendix 2), revealed ten possible homozygous mutations (Appendix 3), only one of which was in a gene (*TULP1*) known to cause RP [16]. This variant, a homozygous missense mutation (NC_000006:g.35471576G>A; NM_003322:c.1162C>T; NP_003313:p.Pro388Ser) in exon 12 of the *TULP1* gene, results in a substitution of proline by serine in a conserved amino acid position (Figure 2B). Aside from the potentially pathogenic mutation in *TULP1*, the only known pathogenic mutation (p.Arg89His) that was identified in the affected individual was in the *INS* gene (Gene ID: 3630, OMIM: 176730; Appendix 4), which is associated with hyperproinsulinemia, a disease not known to result in the described ocular phenotype [18]. Nonetheless, the P388S *TULP1* mutation is a novel variant absent from the 1000 Genomes Project database, the Genome Aggregation Database (v2.1.1), the TOPMed database (freeze 5), and the GenomeAsia 100 K Project database [19]. Segregation of the variant in the consanguineous pedigree was examined with Sanger sequencing to reveal that the parents are heterozygous for the mutation (Figure 2A, Appendix 5). P388 is a highly conserved residue among the species tested, including mammals (Figure 2B) with a $GERP^{2+}$ score [20] of 4.95 (Figure 2C). In silico prediction indicates that the change to proline at this position could

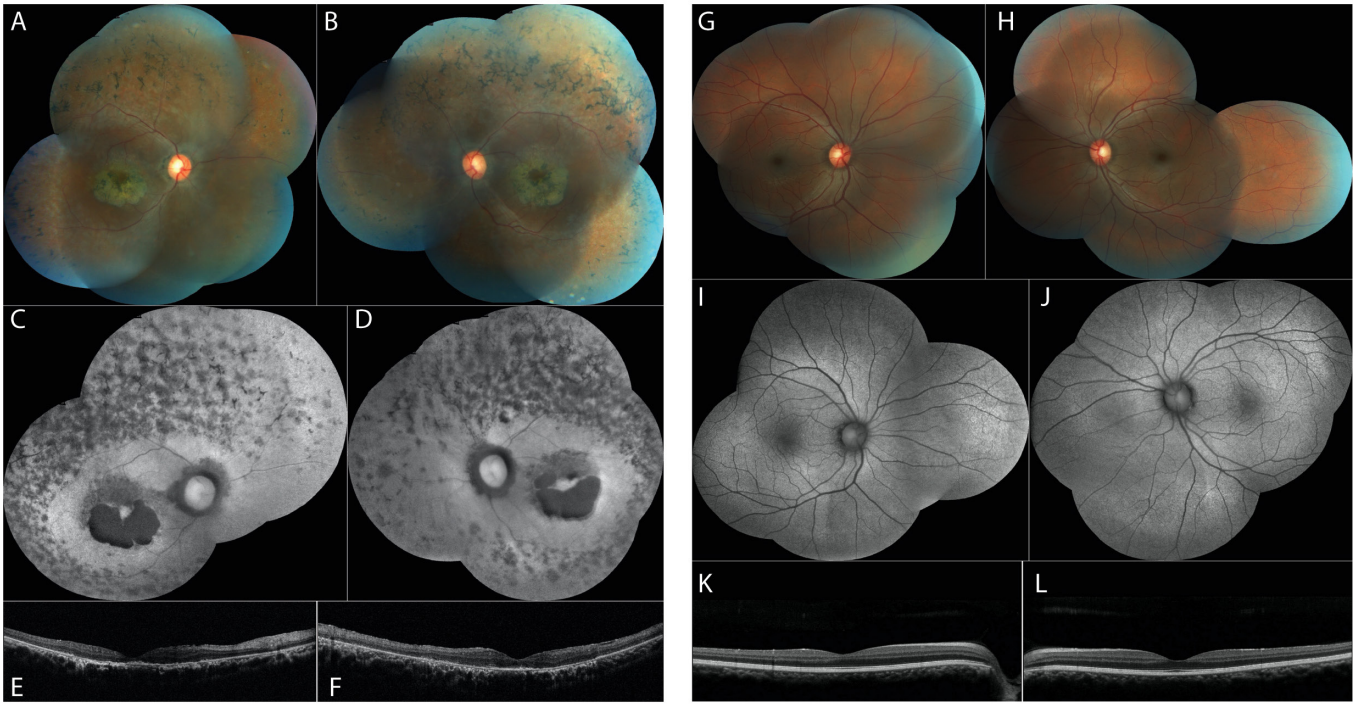

Figure 1. Clinical characterization of the patient. **A, B**: Fundus photographs of the patient's right and left eyes showing parafoveal RPE atrophy, bone spicule-like pigmentation, and arteriolar attenuation. **C, D**: Fundus autofluorescence images showing parafoveal hypoautofluorescence corresponding to the area of RPE atrophy and a patchy decrease in autofluorescence throughout the retina in both eyes. **E, F**: Optical coherence tomography (OCT) scans through the macula showing outer retinal atrophy with loss of the ellipsoid zone. **G**–**L**: Fundus photographs, autofluorescence, and OCT images of an age-matched control subject.

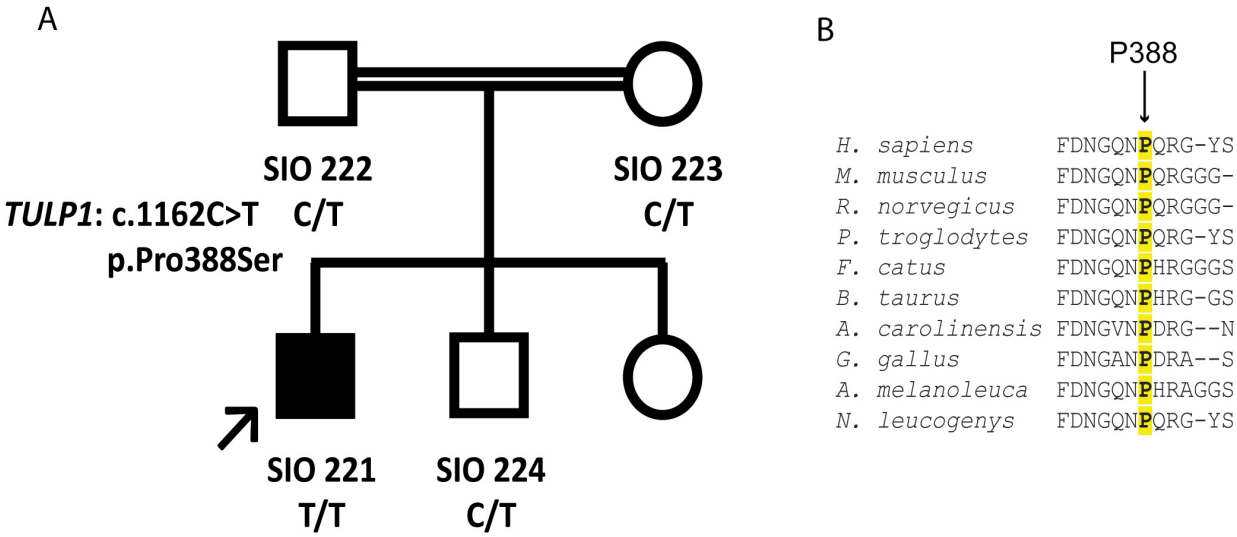

C

	GERP^{++}	CADD	PolyPhen-2	PROVEAN
P388S TULP1	4.95	26.9	0.997	-7.9
			probably damaging	deleterious

Figure 2. Pedigree and in silico analysis of the pathogenic mutation. **A**: Pedigree of the consanguineous family with variant segregation based on Sanger sequencing. **B**: Multiple sequence alignment of TULP1 amino acid residues across species. Arrow indicates highlighted TULP1 residue. Alignments were performed using Clustal Omega multiple sequence alignment software. **C**: In silico prediction findings related to the P388S mutation.

possibly perturb protein function or contribute to pathogenicity with a PolyPhen-2 score [6] of 0.997 (probably damaging), a CADD score [21] of 26.9, and a PROVEAN score [22] of −7.9 (deleterious). Analysis of known mutations in *TULP1* showed an enrichment of mutations occurring in the C-terminus of TULP1 (> amino acid 300), with P338S falling within this region (Appendix 6).

P388S displays similar subcellular localization to WT TULP1: Previously, WT TULP1 has been shown to localize near the plasma membrane and in the nuclear compartments of COS-7 cells [23]. A separate study suggested that missense mutations in TULP1 shift its sub-cellular trafficking, resulting in ER localization [13]. Therefore, we tested whether the P388S mutant displayed localization differences compared to WT TULP1 in cultured cells. HEK-293A cells (STR verified, Appendix 1) were transiently transfected with eGFP, WT TULP1 eGFP, or P388S TULP1 eGFP constructs and analyzed for green fluorescence and counterstained with phalloidin, which binds to F-actin, using laser-scanning confocal microscopy (Figure 3A–C). As expected, expression of eGFP showed the fluorescent signal distributed evenly across the cytoplasm in cells (Figure 3A). WT TULP1 eGFP was localized near the plasma membrane as well as in the nuclear compartments of cells (Figure 3B) similar to previous reports in COS-7 cells [11,23]. Surprisingly, we found that localization of P388S TULP1 eGFP was similar to that of WT TULP1 eGFP in that it also localized predominantly near the plasma membrane and in the nuclear compartment of cells (Figure 3C), suggesting that there are no differences in cellular distribution between WT and P388S TULP1. To confirm that these observations were not cell type-dependent, we also transfected human immortalized RPE (ARPE-19) cells (also STR verified, Appendix 1) with the constructs indicated above and observed that P388S TULP1 eGFP again localized similarly to WT TULP1 eGFP in the nucleus and near the plasma membrane of the cells (Appendix 7).

Protein expression and solubility of P388S TULP1: Because we did not detect obvious differences between WT and P388S TULP1 at the sub-cellular level, we investigated other potential biochemical differences that might partially explain the RP phenotype observed in the patient with the presumed pathogenic variant, p.Pro388Sser in *TULP1*. We employed

a biochemical approach to detect the expression and solubility of WT and P388S TULP1. Using HEK-293A cells, we transfected WT TULP1 eGFP and P388S TULP1 eGFP, and isolated the soluble and insoluble protein fractions from the cells 24 h later. WT TULP1 eGFP and P388S TULP1 eGFP in the soluble and insoluble fractions migrated as predicted at a molecular weight of about 100 kDa (Figure 4A, TULP1 is about 70 kDa [12], and eGFP is about 26–28 kDa [24]). WT TULP1 and P388S TULP1 were similarly more abundant in the RIPA-soluble fraction, as expected based on previous findings [12] (Figure 4A). However, we detected a significant 27.7±13.8% and 22.2±12.4% decrease in soluble and insoluble P388S TULP1 protein levels compared to WT TULP1, respectively (Figure 4B). Furthermore, these observed differences were not due to variations at the transcript level, as qPCR revealed no statistically significant difference between WT and P388S *TULP1* (Figure 4C).

P388S is degraded more rapidly than WT TULP1: Because we observed a significant reduction in P388S TULP1 protein steady-state levels compared to WT TULP1 (Figure 3A,B), we hypothesized that this may indicate that P388S TULP1 is less stable in vitro. To more definitively address whether there were any differences in stability at the protein level between WT TULP1 and P388S TULP1, transfected HEK-293A cells were treated with cycloheximide (CHX), a translation elongation inhibitor, over the course of 9 h. With western blotting, we observed a gradual decrease in protein levels for WT and P388S TULP1 under CHX treatment over time (Figure 5A,B). Initially, we observed an 18.4±18.2% reduction in P388S levels, compared to a 4.8±5.5% reduction in WT TULP1

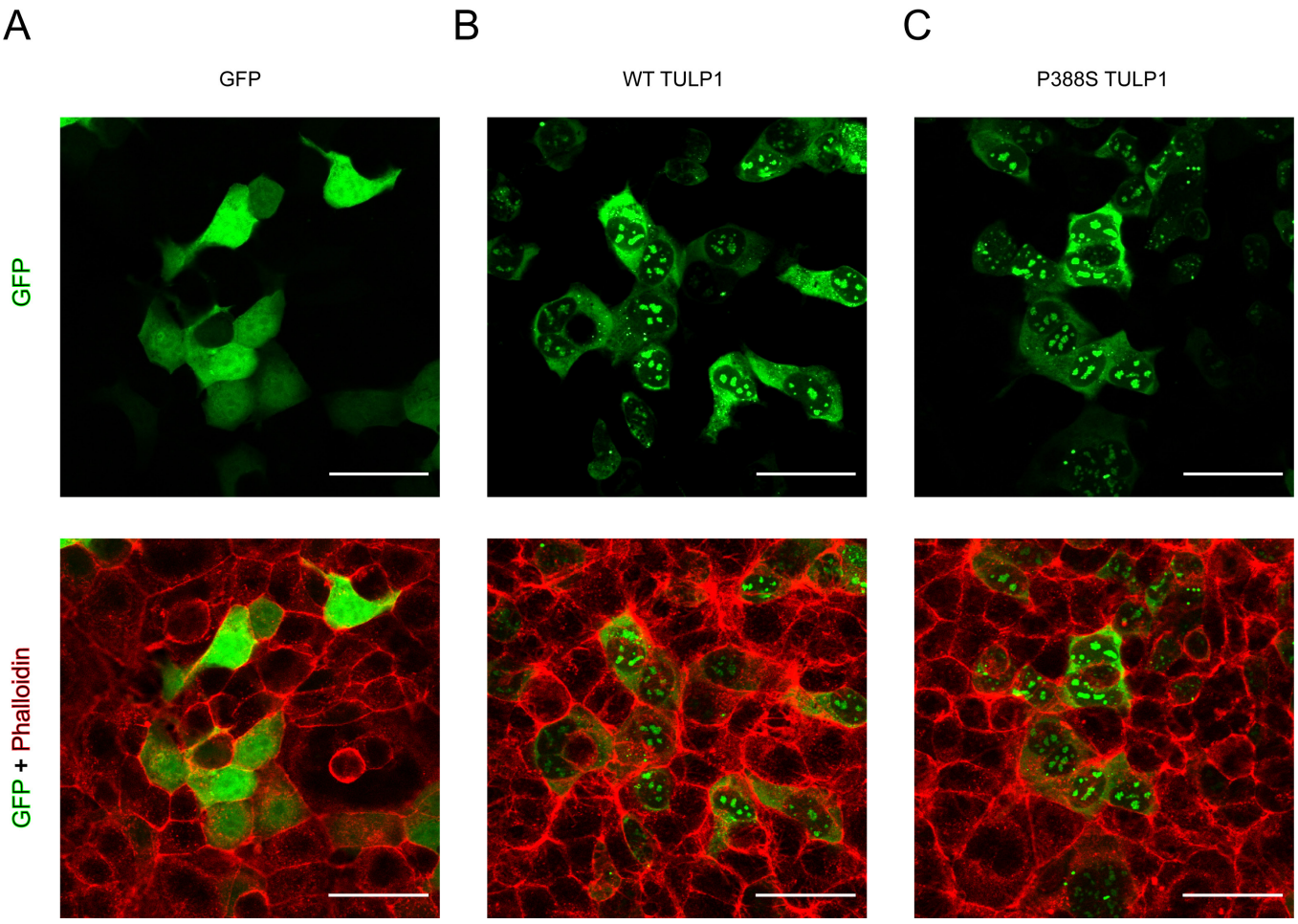

Figure 3. Sub-cellular localization of WT TULP1 and P388S TULP1. Representative confocal microscopy images of human embryonic kidney (HEK-293A) cells transfected with (**A**) green fluorescent protein (peGFP-C1), **B**: wild-type (WT) TULP1 enhanced GFP (eGFP), or (**C**) P388S TULP1 eGFP constructs (green) and stained with AlexaFluor 633 phalloidin (red). Scale bar = 50 µm. TULP1 eGFP images are representative n≥5 biologic, independent replicates. Phalloidin images were representative of n≥3 separate independent wells of a single transfection experiment.

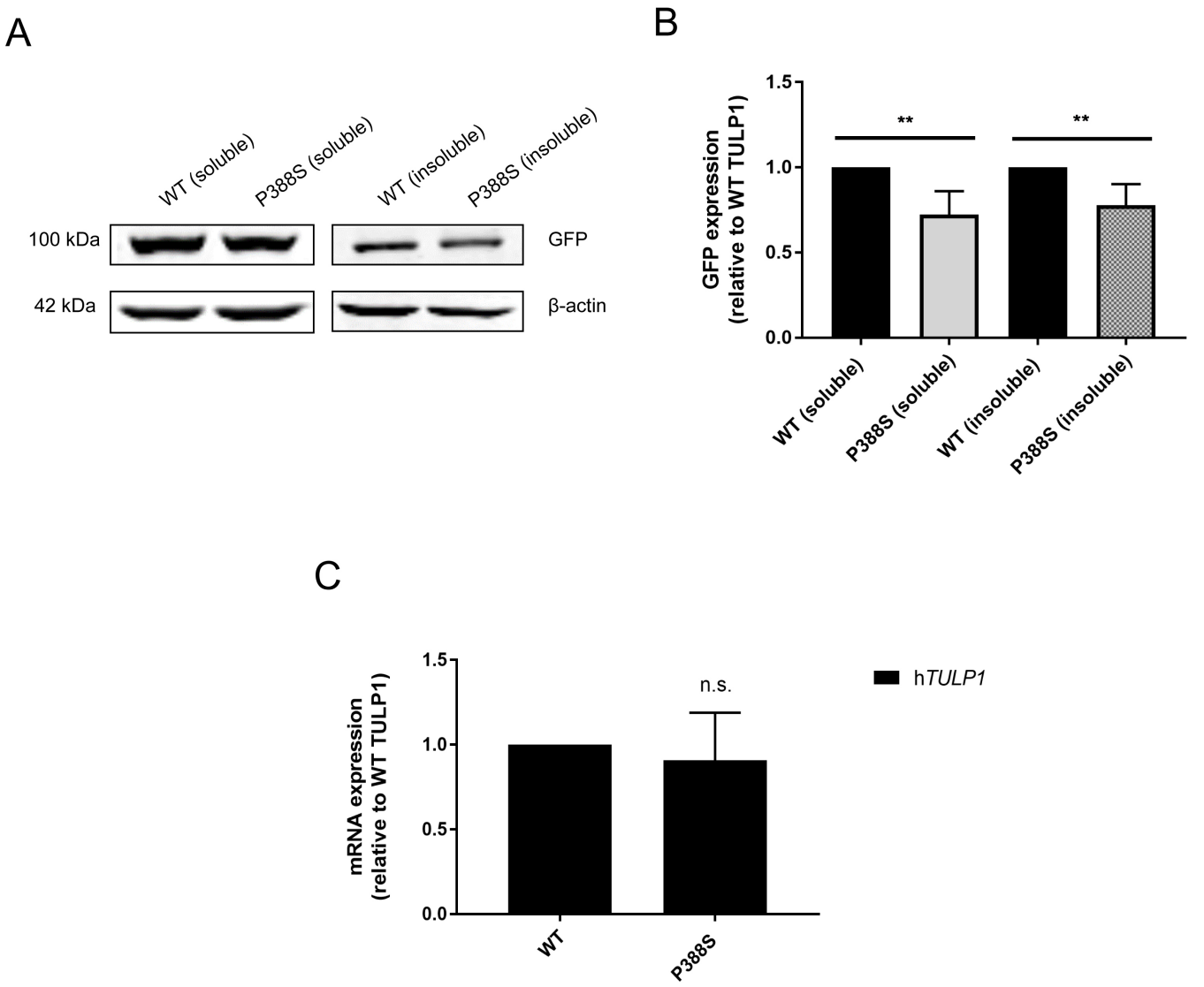

Figure 4. Characterization of the P388S TULP1 variant. **A**: Western blot of wild-type (WT) and P388S TULP1 enhanced green fluorescent protein (eGFP) levels in soluble and insoluble fractions. **B**: Quantification of WT and P388S TULP1 eGFP expression in soluble and insoluble fractions of western blot in (**A**), n≥5, mean ± standard deviation (SD; **p<0.01, one-sample *t* test versus hypothetical value of 1 [i.e., unchanged]). **C**: Quantitative PCR (qPCR) of TULP1 mRNA expression from WT TULP1 eGFP- and P388S TULP1 eGFP-transfected HEK-293A cells. Representative data of n≥3 independent experiments, mean ± SD; n.s., not significant.

after 1 h of treatment with CHX (25 µM, Figure 5A–C, not statistically significant). After 3 h of CHX treatment, we observed a statistically significant 48.7±7.90% reduction in P388S levels, in contrast to the stability of WT TULP1 (5.00±12.3%, Figure 5A–C, p<0.01, *t* test), indicating that P388S is more rapidly degraded at this time point. Finally, at 9 h, we detected a 74.1±11.6% reduction in P388S, whereas WT TULP1 displayed only a 53.6±3.10% reduction in protein levels (Figure 5A–C, p<0.05, *t* test). These data suggest that P388S is generally more unstable and has a higher turnover rate compared to WT TULP1.

P388S TULP1 does not induce ER stress: Missense mutations in *TULP1* have been shown to induce ER stress in vitro [13]. Similarly, we hypothesized that P388S TULP1 may also induce ER stress in cells. To test this hypothesis, we transfected HEK-293A cells and performed qPCR using TaqMan probes that are representative downstream genes of unfolded protein response (UPR) pathway activation [25]. To measure changes in ER stress, we selected the heat shock protein 70

family protein 5 (*HSPA5*, *ATF6* activation, Gene ID: 3309, OMIM: 138120), DnaJ homolog subfamily B member 9 (*DNAJB9*, *IRE1* activation, Gene ID: 4189, OMIM: 602634), and asparagine synthetase (*ASNS*, *PERK* activation, Gene ID: 440, OMIM: 108370) genes. We measured the mRNA expression levels of each gene in HEK-293A cells expressing either WT or P388S TULP1 and detected no statistically significant differences in the *HSPA5*, *DNAJB9*, and *ASNS* transcript levels (Figure 6A), suggesting that the presence of P388S does not induce ER stress within cells. We also confirmed these observations at the protein level by analyzing the GRP78 (*HSPA5*) levels (Figure 6B,C). We found that P388S did not induce statistically significant cellular stress in cultured cells when compared to WT TULP1. These results suggest that the P388S TULP1 variant likely contributes to RP by an alternate mechanism other than ER stress.

DISCUSSION

More than 25 mutations in *TULP1* have been implicated in RP and Leber congenital amaurosis (LCA), including splice-site, frameshift, nonsense, and missense mutations [8,26-32] (Appendix 6). In the present study, we characterized the P388S TULP1 variant found in an individual with autosomal recessive RP.

When monitoring TULP1 sub-cellular localization in HEK-293A and ARPE-19 cells, as well as ER stress markers as a consequence of *TULP1* expression, we found no obvious differences between WT TULP1- or P388S TULP1-expressing cells. These observations are in contrast to a previous report showing that missense mutations in *TULP1* can induce ER stress in cultured cells [13]. The present study results suggest that not all mutations in *TULP1*

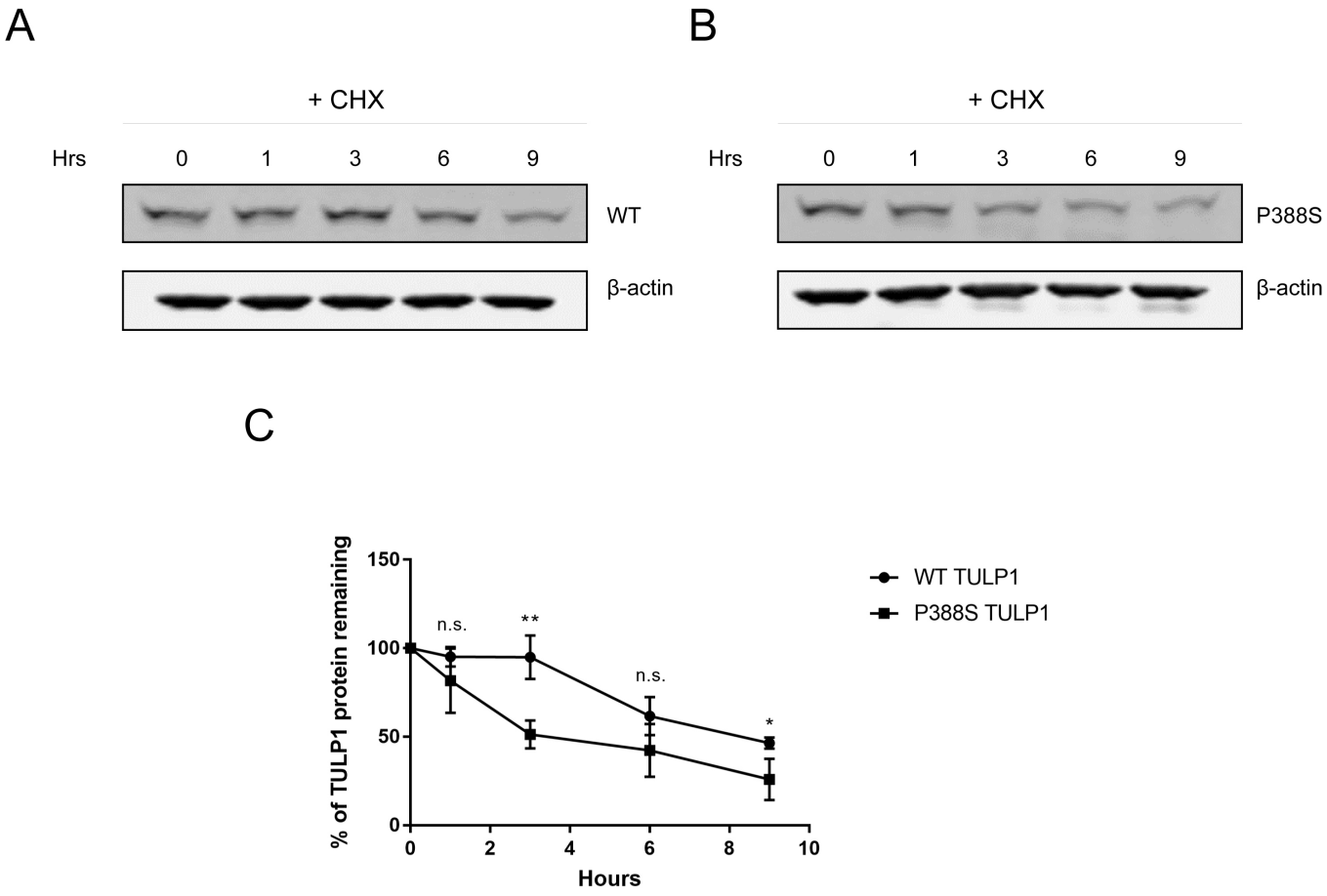

Figure 5. Cycloheximide chase of WT and P388S TULP1. **A, B**: Western blots of wild-type (WT) and P388S TULP1 enhanced green fluorescent protein (eGFP) stability in human embryonic kidney (HEK)-293A cells treated with 25 µM cycloheximide (CHX) and harvested at the indicated time points. **C**: Quantification of western blot from (**A**) and (**B**) showing percentage of TULP1 remaining over time when treated with CHX. (●) indicates WT TULP1 eGFP, and (■) indicates P388S TULP1 eGFP. n = 3 independent experiments, mean ± standard deviation (SD); *p<0.05, **p<0.01, two-tailed *t* test compared to each WT value, n.s., not significant.

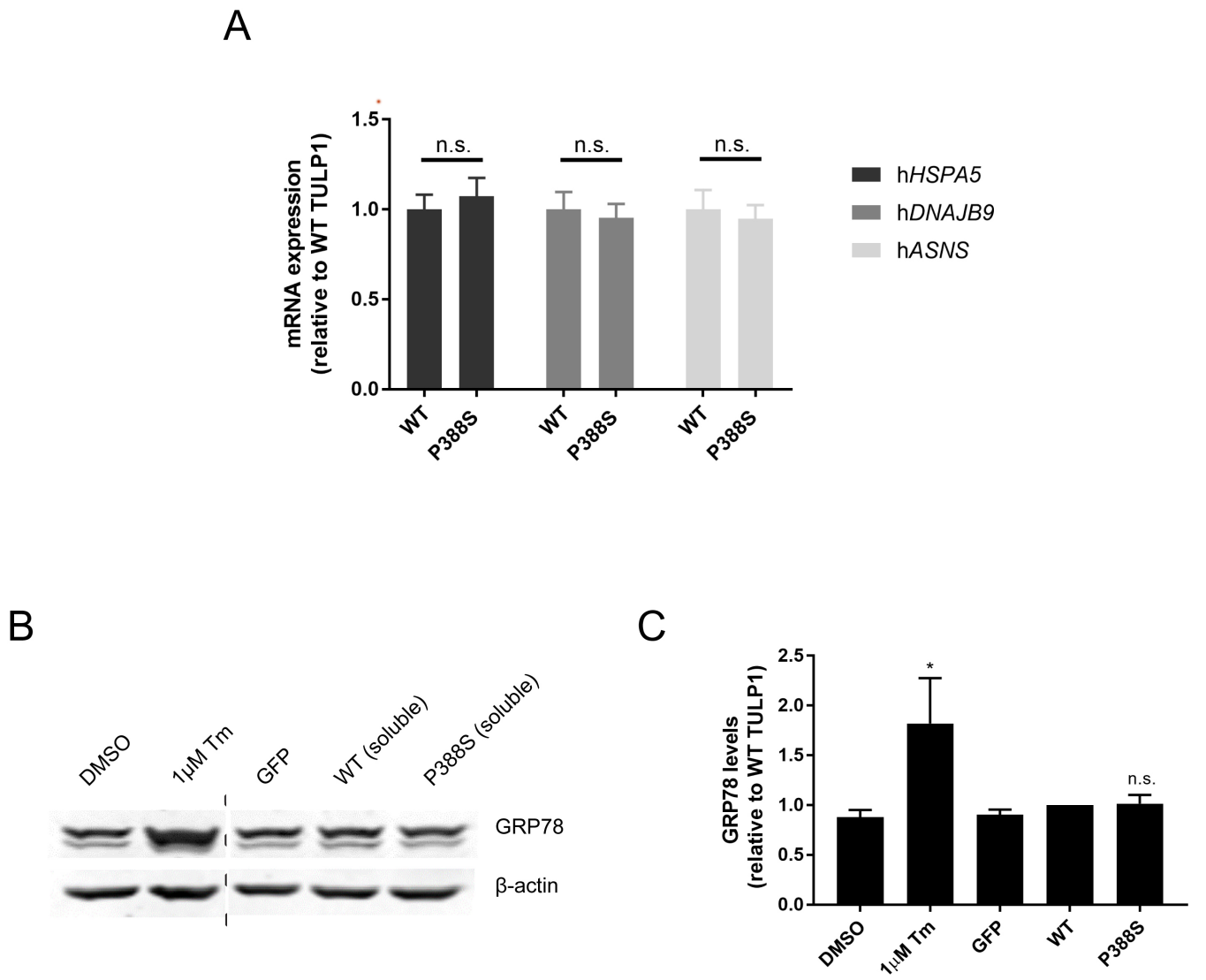

Figure 6. P388S TULP1 does not activate the ER stress response. **A**: Quantitative PCR (qPCR) of *hHSPA5*, *hDNAJB9*, and *hASNS* transcript levels with TaqMan probes in wild-type (WT) TULP1 enhanced green fluorescent protein- (eGFP-) or P388S TULP1 eGFP-expressing cells. **B**: Western blot showing GRP78 expression in eGFP-, WT TULP1 eGFP-, or P388S TULP1 eGFP-transfected cells. One microgram per milliliter Tm was used as a positive control to analyze GRP78 induction. **C**: Quantification of western blot in (**B**). n = 3 biologic independent experiments, mean ± standard deviation (SD); *p<0.05, **p<0.01, one-sample *t* test versus hypothetical value of 1 (i.e., unchanged), n.s., not significant.

induce cellular stress that could potentially lead to disease. In cultured HEK-293A cells, we showed that in comparison to WT TULP1, the P388S mutant protein is unstable and has a faster turnover. Additional RP-associated mutations in *TULP1* (R311Q and R342Q) were also speculated to cause destabilization of the protein in separate studies [33]. Furthermore, upon closer examination of previous data [13], although not specifically elaborated upon in that particular publication, two other mutations in *TULP1*, I459K and F491L, also appear to show a greater than or equal to 45% reduction in apparent steady-state levels relative to WT TULP1. Although largely speculative, the culmination of these results suggest that a reduction in protein stability might be a phenomenon shared among particular *TULP1* variants.

The extent of reduction in protein stability or steady-state levels (on average, about 25%) may not fully explain how the P388S *TULP1* mutation causes RP, but this observation indicates that the protein is likely partially misfolded and may

be nonfunctional. To address this possibility, an ideal experiment would be to introduce P388S TULP1 into *Tulp1−/−* mice to determine whether it can compensate for the loss of *Tulp1,* which is beyond the scope of this study. Nonetheless, the present findings suggest the possibility of another avenue other than ER stress by which select mutations in *TULP1* may lead to disease, and support the idea that evaluation of TULP1 protein stability should be considered when characterizing newly identified mutations in TULP1 associated with RP in vitro.

APPENDIX 1. DEMONSTRATION OF STR VERIFICATION OF THE 293A AND ARPE-19 CELL LINES.

To access the data, click or select the words "Appendix 1." Note that STR verification cannot distinguish among different variants of the 293-based cell lines (i.e., 293 versus 293A versus 293T).

APPENDIX 2. FLOWCHART OF EXOME SEQUENCING PARAMETERS USED TO IDENTIFY PATHOGENIC RECESSIVE MUTATIONS IN RP.

To access the data, click or select the words "Appendix 2."

APPENDIX 3. TEN GENES IDENTIFIED IN THE PROBAND WERE FOUND TO BE IN ACCORDANCE WITH AUTOSOMAL RECESSIVE INHERITANCE.

To access the data, click or select the words "Appendix 3." Of these genes, *TULP1* was identified as the only RP-associated potentially pathogenic gene.

APPENDIX 4. IDENTIFICATION OF THE ARG89HIS KNOWN PATHOGENIC VARIANT IN THE *INS* GENE IN THE PROBAND.

To access the data, click or select the words "Appendix 4."

APPENDIX 5. DNA SEQUENCING CHROMATOGRAM ANALYSIS OF *TULP1* VARIANT IN PROBAND AND FAMILY MEMBERS.

To access the data, click or select the words "Appendix 5."

APPENDIX 6. KNOWN MUTATIONS IN *TULP1* IDENTIFIED IN PATIENTS WITH RP OR LCA.

To access the data, click or select the words "Appendix 6."

APPENDIX 7. SUB-CELLULAR LOCALIZATION OF WT TULP1 AND P388S TULP1 IN ARPE-19 CELLS.

To access the data, click or select the words "Appendix 7." Representative confocal microscopy images of ARPE-19 cells transfected with (*A*) peGFP-C1, (*B*) WT TULP1 eGFP, or (*C*) P388S TULP1 eGFP constructs. GFP signal is detected in cytoplasm and/or nucleus. The nuclei were stained with 4,6-diamidino-2-phenylindole, dilactate (DAPI; blue). Scale bar=20µm. Representative images from n=4 biologic, independent replicates.

ACKOWLEDGEMENTS

DRW is supported by an NIH Diversity Supplement (R01EY027785). JDH is supported by an endowment from the Roger and Dorothy Hirl Research Fund, an NEI R01 grant (R01EY027785), and a Career Development Award from Research to Prevent Blindness (RPB). Additional support was provided by an NEI Visual Science Core grant (P30EY030413) and an unrestricted grant from RPB (both to the UT Southwestern Department of Ophthalmology). Dr. Hulleman (John.Hulleman@UTSouthwestern.edu) and Dr. Mootha (Vinod.Mootha@UTSouthwestern.edu) are co-corresponding authors for this paper. We would like to thank the patient and his family for participating in this study.

REFERENCES

1. Sahel JA, Marazova K, Audo I. Clinical characteristics and current therapies for inherited retinal degenerations. Cold Spring Harb Perspect Med 2014; 5:a017111-[PMID: 25324231].
2. Hamel CP. Cone rod dystrophies. Orphanet J Rare Dis 2007; 2:7-[PMID: 17270046].
3. Hamel C. Retinitis pigmentosa. Orphanet J Rare Dis 2006; 1:40-[PMID: 17032466].
4. Ferrari S, Di Iorio E, Barbaro V, Ponzin D, Sorrentino FS, Parmeggiani F. Retinitis pigmentosa: genes and disease mechanisms. Curr Genomics 2011; 12:238-49. [PMID: 22131869].
5. Ullah I, Kabir F, Iqbal M, Gottsch CB, Naeem MA, Assir MZ, Khan SN, Akram J, Riazuddin S, Ayyagari R, Hejtmancik JF, Riazuddin SA. Pathogenic mutations in TULP1 responsible for retinitis pigmentosa identified in consanguineous familial cases. Mol Vis 2016; 22:797-815. [PMID: 27440997].
6. Adzhubei IA, Schmidt S, Peshkin L, Ramensky VE, Gerasimova A, Bork P, Kondrashov AS, Sunyaev SR. A method and server for predicting damaging missense mutations. Nat Methods 2010; 7:248-9. [PMID: 20354512].
7. Paloma E, Hjelmqvist L, Bayes M, Garcia-Sandoval B, Ayuso C, Balcells S, Gonzalez-Duarte R. Novel mutations in the

TULP1 gene causing autosomal recessive retinitis pigmentosa. Invest Ophthalmol Vis Sci 2000; 41:656-9. [PMID: 10711677].

8. Iqbal M, Naeem MA, Riazuddin SA, Ali S, Farooq T, Qazi ZA, Khan SN, Husnain T, Riazuddin S, Sieving PA, Hejtmancik JF, Riazuddin S. Association of pathogenic mutations in TULP1 with retinitis pigmentosa in consanguineous Pakistani families. Arch Ophthalmol 2011; 129:1351-7. [PMID: 21987678].

9. Milam AH, Hendrickson AE, Xiao M, Smith JE, Possin DE, John SK, Nishina PM. Localization of tubby-like protein 1 in developing and adult human retinas. Invest Ophthalmol Vis Sci 2000; 41:2352-6. [PMID: 10892883].

10. Hagstrom SA, Adamian M, Scimeca M, Pawlyk BS, Yue G, Li T. A role for the Tubby-like protein 1 in rhodopsin transport. Invest Ophthalmol Vis Sci 2001; 42:1955-62. [PMID: 11481257].

11. Xi Q, Pauer GJ, Marmorstein AD, Crabb JW, Hagstrom SA. Tubby-like protein 1 (TULP1) interacts with F-actin in photoreceptor cells. Invest Ophthalmol Vis Sci 2005; 46:4754-61. [PMID: 16303976].

12. Hagstrom SA, Duyao M, North MA, Li T. Retinal degeneration in tulp1−/− mice: vesicular accumulation in the interphotoreceptor matrix. Invest Ophthalmol Vis Sci 1999; 40:2795-802. [PMID: 10549638].

13. Lobo GP, Au A, Kiser PD, Hagstrom SA. Involvement of Endoplasmic Reticulum Stress in TULP1 Induced Retinal Degeneration. PLoS One 2016; 11:e0151806-[PMID: 26987071].

14. McKenna A, Hanna M, Banks E, Sivachenko A, Cibulskis K, Kernytsky A, Garimella K, Altshuler D, Gabriel S, Daly M, DePristo MA. The Genome Analysis Toolkit: a MapReduce framework for analyzing next-generation DNA sequencing data. Genome Res 2010; 20:1297-303. [PMID: 20644199].

15. Cingolani P, Platts A. Wang le L, Coon M, Nguyen T, Wang L, Land SJ, Lu X, Ruden DM. A program for annotating and predicting the effects of single nucleotide polymorphisms, SnpEff: SNPs in the genome of Drosophila melanogaster strain w1118; iso-2; iso-3. Fly (Austin) 2012; 6:80-92. [PMID: 22728672].

16. Martin-Merida I, Avila-Fernandez A, Del Pozo-Valero M, Blanco-Kelly F, Zurita O, Perez-Carro R, Aguilera-Garcia D, Riveiro-Alvarez R, Arteche A, Trujillo-Tiebas MJ, Tahsin-Swafiri S, Rodriguez-Pinilla E, Lorda-Sanchez I, Garcia-Sandoval B, Corton M, Ayuso C. Genomic Landscape of Sporadic Retinitis Pigmentosa: Findings from 877 Spanish Cases. Ophthalmology 2019; 126:1181-8. [PMID: 30902645].

17. Hulleman JD, Nguyen A, Ramprasad VL, Murugan S, Gupta R, Mahindrakar A, Angara R, Sankurathri C, Mootha VV. A novel H395R mutation in MKKS/BBS6 causes retinitis pigmentosa and polydactyly without other findings of Bardet-Biedl or McKusick-Kaufman syndrome. Mol Vis 2016; 22:73-81. [PMID: 26900326].

18. Gruppuso PA, Gorden P, Kahn CR, Cornblath M, Zeller WP, Schwartz R. Familial hyperproinsulinemia due to a proposed defect in conversion of proinsulin to insulin. N Engl J Med 1984; 311:629-34. [PMID: 6382002].

19. . GenomeAsia KC. The GenomeAsia 100K Project enables genetic discoveries across Asia. Nature 2019; 576:106-11. [PMID: 31802016].

20. Davydov EV, Goode DL, Sirota M, Cooper GM, Sidow A, Batzoglou S. Identifying a high fraction of the human genome to be under selective constraint using GERP++. PLOS Comput Biol 2010; 6:e1001025-[PMID: 21152010].

21. Kircher M, Witten DM, Jain P, O'Roak BJ, Cooper GM, Shendure J. A general framework for estimating the relative pathogenicity of human genetic variants. Nat Genet 2014; 46:310-5. [PMID: 24487276].

22. Choi Y, Chan AP. PROVEAN web server: a tool to predict the functional effect of amino acid substitutions and indels. Bioinformatics 2015; 31:2745-7. [PMID: 25851949].

23. He W, Ikeda S, Bronson RT, Yan G, Nishina PM, North MA, Naggert JK. GFP-tagged expression and immunohistochemical studies to determine the subcellular localization of the tubby gene family members. Brain Res Mol Brain Res 2000; 81:109-17. [PMID: 11000483].

24. Arpino JA, Rizkallah PJ, Jones DD. Crystal structure of enhanced green fluorescent protein to 1.35 A resolution reveals alternative conformations for Glu222. PLoS One 2012; 7:e47132-[PMID: 23077555].

25. Hulleman JD, Brown SJ, Rosen H, Kelly JW. A high-throughput cell-based Gaussia luciferase reporter assay for identifying modulators of fibulin-3 secretion. J Biomol Screen 2013; 18:647-58. [PMID: 23230284].

26. den Hollander AI, Lopez I, Yzer S, Zonneveld MN, Janssen IM, Strom TM, Hehir-Kwa JY, Veltman JA, Arends ML, Meitinger T, Musarella MA, van den Born LI, Fishman GA, Maumenee IH, Rohrschneider K, Cremers FP, Koenekoop RK. Identification of novel mutations in patients with Leber congenital amaurosis and juvenile RP by genome-wide homozygosity mapping with SNP microarrays. Invest Ophthalmol Vis Sci 2007; 48:5690-8. [PMID: 18055821].

27. Kannabiran C, Singh H, Sahini N, Jalali S, Mohan G. Mutations in TULP1, NR2E3, and MFRP genes in Indian families with autosomal recessive retinitis pigmentosa. Mol Vis 2012; 18:1165-74. [PMID: 22605927].

28. Abbasi AH, Garzozi HJ, Ben-Yosef T. A novel splice-site mutation of TULP1 underlies severe early-onset retinitis pigmentosa in a consanguineous Israeli Muslim Arab family. Mol Vis 2008; 14:675-82. [PMID: 18432314].

29. Hagstrom SA, North MA, Nishina PL, Berson EL, Dryja TP. Recessive mutations in the gene encoding the tubby-like protein TULP1 in patients with retinitis pigmentosa. Nat Genet 1998; 18:174-6. [PMID: 9462750].

30. RetNet, the Retinal Information Network. August 27, 2019]; Available from: https://sph.uth.edu/RetNet/

31. den Hollander AI, van Lith-Verhoeven JJ, Arends ML, Strom TM, Cremers FP, Hoyng CB. Novel compound heterozygous TULP1 mutations in a family with severe early-onset retinitis

pigmentosa. Arch Ophthalmol 2007; 125:932-5. [PMID: 17620573].

32. Lewis CA, Batlle IR, Batlle KG, Banerjee P, Cideciyan AV, Huang J, Aleman TS, Huang Y, Ott J, Gilliam TC, Knowles JA, Jacobson SG. Tubby-like protein 1 homozygous splice-site mutation causes early-onset severe retinal degeneration. Invest Ophthalmol Vis Sci 1999; 40:2106-14. [PMID: 10440267].

33. Hebrard M, Manes G, Bocquet B, Meunier I, Coustes-Chazalette D, Herald E, Senechal A, Bolland-Auge A, Zelenika D, Hamel CP. Combining gene mapping and phenotype assessment for fast mutation finding in non-consanguineous autosomal recessive retinitis pigmentosa families. European journal of human genetics Eur J Hum Genet 2011; 19:1256-63. [PMID: 21792230].

Articles are provided courtesy of Emory University and the Zhongshan Ophthalmic Center, Sun Yat-sen University, P.R. China. The print version of this article was created on 2 April 2021. This reflects all typographical corrections and errata to the article through that date. Details of any changes may be found in the online version of the article.